JSBS Journal of Sistan and Baluchistan Studies
Volume 6, Issue 1 (2026) 35-52
Doi: 10.22034/jsbs.2025.534785.1099

BENEATH THE ANCIENT PATINA: INSIGHTS INTO THE CHARACTERIZING AND ARCHAEOMETALLURGY OF SOME BRONZE AGE COPPER-ARSENIC ARTIFACTS FROM SHAHR-I SOKHTA (SOUTHEAST IRAN)

Vahid POURZAGHAN [1], **Hamidreza BAKHSHANDEHFARD** [2] ✉, **Mahmoud ABDELLATIEF** [3], **Mohammadamin EMAMI** [4]

[1] Department of Conservation of Historical Objects and Archaeometry, Faculty of Conservation and Restoration, Art University of Isfahan, Isfahan, Iran.
[2] Department of Conservation of Historical Objects and Archaeometry, Faculty of Conservation and Restoration, Art University of Isfahan, Isfahan, Iran, (hr.bakhshan@aui.ac.ir)
[3] SESAME Synchrotron, King Hussein Bin Talal St / Box 7, Allan, 19252, Jordan.
[4] Department of Conservation of Historical Objects and Archaeometry, Faculty of Conservation and Restoration, Art University of Isfahan, Isfahan, Iran.

Received: 15 July 2025 Accepted: 12 September 2025 Available online: 20 June 2026

Abstract: Shahr-i Sokhta, one of the prominent Bronze Age sites located in the Sistan and Baluchistan province of eastern Iran, houses a valuable collection of metal artifacts. This study investigates the corrosion characteristics and mechanisms affecting copper-arsenic bronze artifacts recovered from both the residential area and cemetery of Shahr-i Sokhta. The main goal is to consider to identify the nature, chemical composition, and physical properties of the corrosion products (patinas) on the surfaces of these artifacts to better understand their archaeometallurgical characterization. The research aims to understand what are the chemical and structural characteristics of the corrosion products, and how these relate to the metallurgical aspects of the artifacts. Additionally, we aim to uncover, what are the mechanisms that govern the corrosion process, and what their role is in determining and identifying manufacturing technology in this regard? In order to identify the answers to these questions, the samples were analyzed using optical microscopy, scanning electron microscopy equipped with energy dispersive X-ray spectroscopy (SEM-EDX), and elemental mapping to analyze their structure and chemical composition. Additionally, synchrotron-based X-ray diffraction (XRD) and X-ray fluorescence (XRF) techniques were applied to identify the corrosion compounds and assess their relationship with the burial soil conditions. The findings of the study demonstrate that the metal artifacts from Shahr-i Sokhta are predominantly composed of Sn–As–Cu alloys, characterized by a relatively low arsenic concentration, averaging approximately 2.77 wt%. Corrosion morphologies suggest internal degradation processes. Soil analysis revealed that the presence of apatite facilitates the migration of arsenic ions. Moreover, the detection of sinnerite, a copper sulfosalt, on the artifact surfaces indicates reductive conditions within the burial environment. These findings contribute to a deeper understanding of the archaeometallurgy and conservation challenges associated with copper-arsenic bronzes at this significant Bronze Age site.
Keywords: Copper-arsenic bronzes, Patina, Corrosion, Shahr-i Sokhta, Archaeometallurgical characterization.

چکیده: شهر سوخته، یکی از محوطه‌های شاخص عصر مفرغ در استان سیستان و بلوچستان در شرق ایران، مجموعه‌ای ارزشمند از مصنوعات فلزی را در خود جای داده است. این پژوهش به بررسی ویژگی‌ها و سازوکارهای خوردگی در مصنوعات مفرغی مس ـ آرسنیک به‌دست‌آمده از بخش‌های مسکونی و گورستان شهر سوخته می‌پردازد. هدف اصلی، شناسایی ماهیت، ترکیب شیمیایی و ویژگی‌های فیزیکی محصولات خوردگی (پتینه‌ها) بر سطح این آثار به‌منظور درک بهتر از ویژگی‌های باستان‌فلزشناسی آنهاست. در این راستا، پژوهش به دنبال پاسخ به این پرسش‌هاست که ترکیب و ساختار شیمیایی محصولات خوردگی چگونه‌اند و این ویژگی‌ها چه نسبتی با جنبه‌های فلزشناسی مصنوعات دارند؟ افزون بر این، پژوهش تلاش دارد سازوکارهای مؤثر در فرایند خوردگی را آشکار سازد و نقش آنها را در تعیین و شناسایی فناوری ساخت این اشیاء تبیین کند. برای پاسخ به این پرسش‌ها، نمونه‌ها با روش‌های میکروسکوپی نوری، میکروسکوپ الکترونی روبشی مجهز به طیف‌سنجی پرتو ایکس (SEM-EDX) و نقشه‌برداری عنصری، از نظر ساختار و ترکیب شیمیایی مورد تجزیه و تحلیل قرار گرفتند. همچنین از روش‌های پراش پرتو ایکس (XRD) و فلورسانس پرتو ایکس (XRF) مبتنی بر سنکروترون برای شناسایی ترکیبات خوردگی و بررسی ارتباط آنها با شرایط خاک تدفینی استفاده شد. یافته‌های پژوهش نشان می‌دهد که مصنوعات فلزی شهر سوخته عمدتاً از آلیاژهای Sn–As–Cu تشکیل شده‌اند که دارای غلظت نسبتاً پایین آرسنیک، با میانگین حدود ۲/۷۷ درصد وزنی، هستند. الگوهای خوردگی نشان‌دهنده وجود فرایندهای تخریب درونی‌اند. تحلیل خاک پیرامون اشیاء بیانگر آن است که حضور آپاتیت، مهاجرت یون‌های آرسنیک را تسهیل می‌کند. همچنین، شناسایی سینریت (یکی از سولفوسالت‌های مس) بر سطح آثار، بیانگر شرایط کاهنده در محیط تدفینی است. این نتایج، درک عمیق‌تری از باستان‌فلزشناسی و چالش‌های حفاظتی مربوط به مفرغ‌های مس ـ ارسنیک در این محوطه مهم عصر مفرغ ارائه می‌دهد.
کلیدواژه: مفرغ‌های مس ـ آرسنیک، پتینه، خوردگی، شهر سوخته، ویژگی‌های باستان‌فلزشناسی.

I. Introduction

The ancient site of Shahr-i Sokhta in Sistan and Baluchistan Province is one of the most important Bronze Age centers located in the southeast of the country, spanning an area of 121 hectares and registered as the 17th UNESCO World Heritage site in 2013. Today's name of *Shahr-i Sokhta* has been devoted since the city suffered from fire in at least two phases of its history. The surface was burnt, and traces of ashes and burns can be seen everywhere; and for this reason, it is called the *Shahr-i Sokhta* (burnt city) by the local people. It was built on the bank of the Hirmand River and Hamon Lake, and on the side of a road in Zabol. The cultural artifact is a real treasure trove of culturally diverse information and data, including pins, rods, mirrors, small seals, and a silver submediant (kohl container rod). The city can be divided into three main parts and three sub-parts, which include the large central area, comprising the eastern and central residential areas and monuments, the northwest area, or the industrial area, and the southern area, or the cemetery area. According to the archaeological contextualization, *Shahr-i Sokhta* is dated 3200 BCE (Early Bronze Age) with four cultural strata (I-IV) and is divided into eleven phases from 0 to 10 phases. Cultural strata have been proposed by Period I, from 3200 to 2800 BC, Period II, from 2800 to 2500 BC, Period III, from 2500 to 2300 BC, and Period IV; dated from 1800 to 1750 BC (Salvatori and Tosi, 2005).

Archaeological investigations by Ernst Herzfeld before the Second World War, followed by Walter Ashlin Fairservis Jr between 1949 and 1951 in Sistan, led to the discovery of hundreds of ancient sites in Sistan and Baluchistan (Fairservis, 1961). Then, in the 1940s, the Italian archaeological mission ISMEO, headed by Giuseppe Tucci and directed by Umberto Scerrato, began conducting research in Sistan. Archaeologists such as Tosi, Piperno, and Salvatore also took part in this project, which continued until the Islamic Revolution. Following the eighteenth excavation season, from 1997 to 2016, these activities were carried out in the region by Seyyed Sajjadi (Tosi, 1984). The works and materials obtained from the graves of this site have helped researchers reach scientific results in various fields. These ancient cultural materials are a real treasure and full of various information and data from a cultural and social point of view (Sajjadi et al., 2003). The corpus includes pins, rods, mirrors, small seals, and vermilion rods, which are severely damaged. The goals of this article are to identify the chemical and structural composition of bronzes uncovered in the area of this site and to determine the stability conditions according to the type of corrosion artifacts from copper-arsenic-based alloys.

Figure 1: Geographical location of *Shahr-i Sokhta* in Sistan and Baluchestan Province, and different parts of the study: residential and cemetery.

II. Materials and Methods

II.1. Material description and collected area

12 samples have been permitted and studied in this research. Regarding the uniqueness of the metals, not all of them might have been considered for analytical studies. 3 samples from the residential area (SS-3, SS-11, SS-12) and 9 samples from the cemetery were analyzed. Samples from the residential area are probably in the form of tools, and the samples from the cemetery have been characterized as broken pieces of jars, including the rims and bodies of the containers and submediant rods. All the objects are likely composed of arsenical copper alloys, a form of bronze. These alloys are regarded as some of the most significant

archaeometallurgical materials from the Early Bronze Age due to their technological importance and widespread use during that period. Since systematic scientific and specialized material research on these works has not been done so far, the forthcoming results can be considered as the base studies for further investigations (Fig. 2, Table 1, and Table 2).

The stratigraphic location of the objects is also shown in Figure 3, illustrating the heterogeneity of the burial environment and the diversity of structural layers. These complex collapses within the stratigraphy may have been caused by fluvial activity along ancient riverbanks. This interpretation is supported by the presence of saline deposits at the base of the trench. Most metallurgical findings from *Shahr-i Sokhta* date to between 2700 and 2500 BC and hold special significance due to their association with the emergence of urbanization in this region.

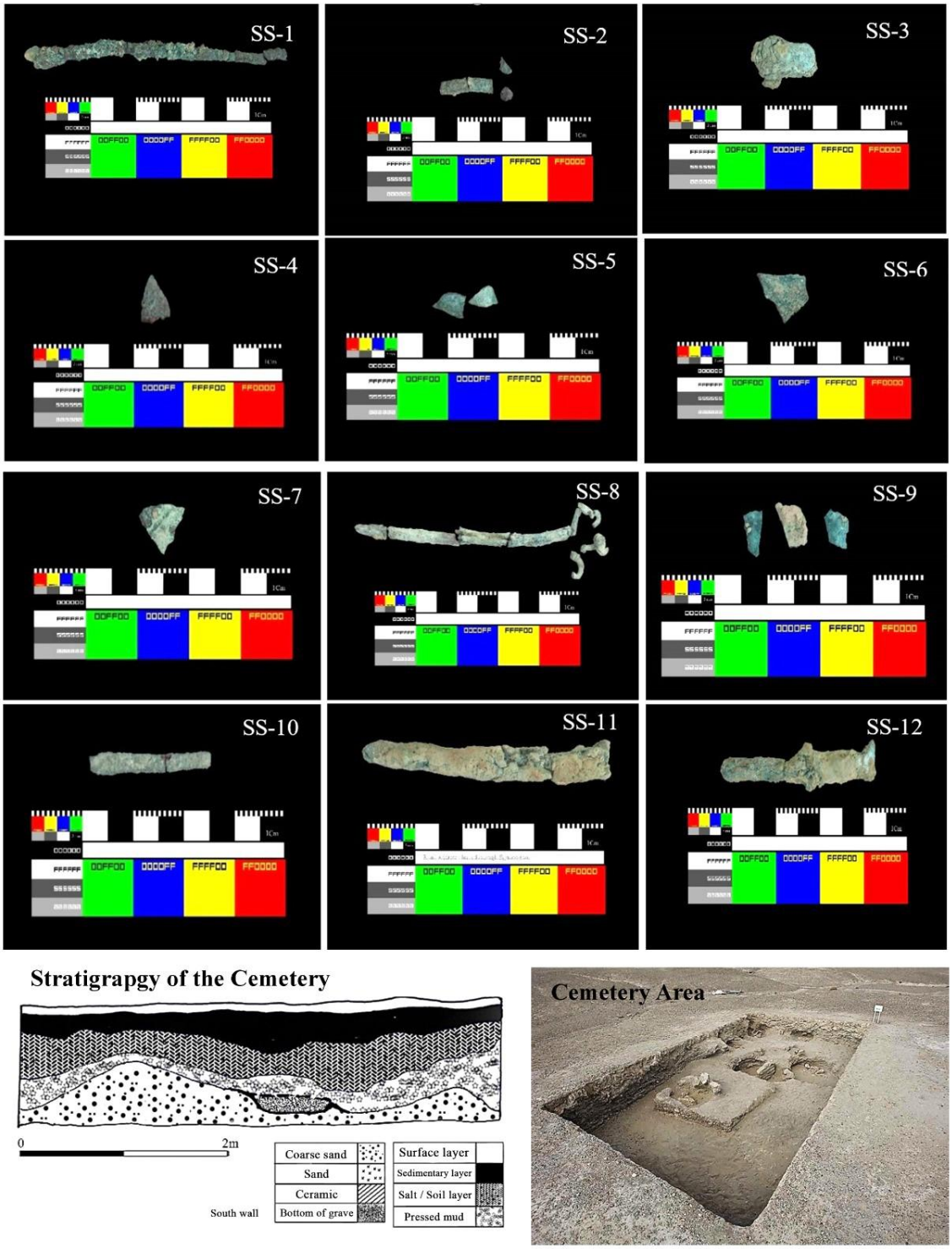

Figure 2: Investigated research samples obtained from the *Shahr-i Sokhta*; samples SS-3, SS-11 and SS-12 are related to the residential area and the other 9 samples are related to the *Shahr-i Sokhta* cemetery. Down left: the stratigraphy of the cemetery, and downright: cemetery trench.

Table 1: The metal artefacts descriptions from the excavations of the cemetery.

Code	Object	Excavat	Borehole	Burial	Excavati	Depth
SS-1	Hairsticks	2002	IUH	3309	9	130
SS-2	Tool	2005	-	-	-	153
SS-4	Probably tool	-	IMG	0335	-	110
SS-5	the edge of the container	-	-	8702	22	165
SS-7	Part of the dish	2009	NFK	8818	1	210
SS-8	Hairsticks		NFP	9002	2	250
SS-9	incense holder base	2009	NFK	8818	4	210
SS-10	Tool	2002	IUR	3200	14	153

Table 2: The metal artefacts discovered from the excavations of the residential area.

Code	Object	Excavation year	Exploration season	Building no	Archaeological exploration workshop	Space number	Section	Depth Cm
SS-3	Figurine	2002	8	5	5	B21	3	130
SS-11	Tool	2007	11	-	5	1	18	122
SS-12	Tool	2007	11	-	5	R1	25	152

II.2. Methods

Bulk chemical analysis was performed using the X-ray fluorescence (XRF) method. For this purpose, approximately 5 grams of corrosion products were carefully collected from the surface of each artifact using a clean, non-contaminating spatula to avoid external contamination. Sampling targeted areas where the corrosion layers were representative of the bulk surface, removing loose, powdery material while minimizing the removal of the underlying metallic core. The depth of collection was controlled to ensure that the sampled material included both corrosion products and any altered metal phases immediately beneath, which is essential for accurate bulk compositional analysis. After collection, the corrosion products from each sample were homogenized to reduce heterogeneity and ensure representativeness. The prepared material was then analyzed using the S4 PIONEER XRF instrument (Bruker, Germany) at the Central Laboratory of Isfahan University, following established archaeometallurgical protocols. This approach allowed reliable determination of the major and minor elemental composition of the corrosion layers, providing insights into the original alloy composition (Robotti et al., 2018). A synchronous-based XRD method was used to determine the composition of the buried soil and identify corrosion products (Abdellatief et al., 2017). High-resolution synchrotron powder X-ray diffraction (XRD) data were collected using the MS beamline [R1, R2] at the SESAME synchrotron facility. The experiments were conducted at a wavelength of 0.82685 Å. The MS beamline operates with a wiggler source and features a double crystal Si(111) Kohzu monochromator, where the second crystal has sagittal bendable horizontal curvature, paired with two Rhodium-coated mirrors for beam conditioning. An ionization chamber in the experimental station monitored the beam flux over time, allowing for scale factor corrections during extended measurements. The setup included a two-circle vertical diffractometer with high-resolution encoders and a Pilatus 300K area detector (172 μm pixel size) positioned 740.4 mm from the sample. The detector covered a 2θ range of 6.4° at this distance. Diffraction patterns were collected in the 2θ range of 1.0° to 60.0°, with each frame captured using a minute exposure time.

FE-SEM, VEGA II TESCAN from the Czech Republic, equipped with X-ray energy diffraction spectrometer (EDX) model Rontec, was used for microstructural investigations at Razi Metallurgical Research Centre. To examine the microstructure and corrosion products, the samples were etched with an alcoholic ferric chloride solution (120 ml ethanol + 30 ml hydrochloric acid + 10 g ferric chloride III) (Scott, 1991) and microscopically examined using a Zeiss instrument, model Primotech.

In order to investigate the burial environment of the samples, soil samples were taken from both the residential area and the cemetery. To determine the moisture content of the soil, 5 grams of soil samples from the ancient site were placed in an oven at 105 degrees Celsius for 24 hours, and the change in weight of the samples was measured. The pH of the soil in both areas was measured using a 744-pH meter from the

United States following the ASTM D4972-01 standard (ASTM D4972-01 2007).

One of the most important corrosion factors in soil and surface environments is electrical conductivity, which plays an important role in the conductivity of dissolved salts and provides an electrolytic environment for corrosion. For this purpose, the electrical conductivity of the soil was measured, SS-Ma1-11, SS-Ma2-12 code for the residential section, and SS-Go1-3 ، SS-Go2-10, SS-Go3-9 for the cemetery section of *Shahr-i Sokhta*. A ratio of 1 to 2 was used for soil to water (Shirokora et al., 2000). The electrical conductivity was measured using an Inolab Terminal 740 conductivity measuring instrument manufactured by WTW in Germany.

III. Results

III.1. Corrosion morphology by Stereo Microscope

Based on observations made with the stereo microscope, the corrosion structures of the samples obtained from *Shahr-i Sokhta* indicate extensive degradation, with some areas being completely corroded. Optically, the presence of CuO in the form of tenorite is evident, characterized by its isotropic properties and dark coloration (SS-1, SS-6 in Fig. 3). Additionally, many samples exhibit a striped morphology, consistent with the Liesegang phenomenon, which reflects periodic precipitation patterns within the corrosion layers (Fig. 3). Micro-chemistry within the corrosion morphology, after SEM studies, approved that in the layers of corrosion products arsenic is irregularly distributed in the form of accumulations.

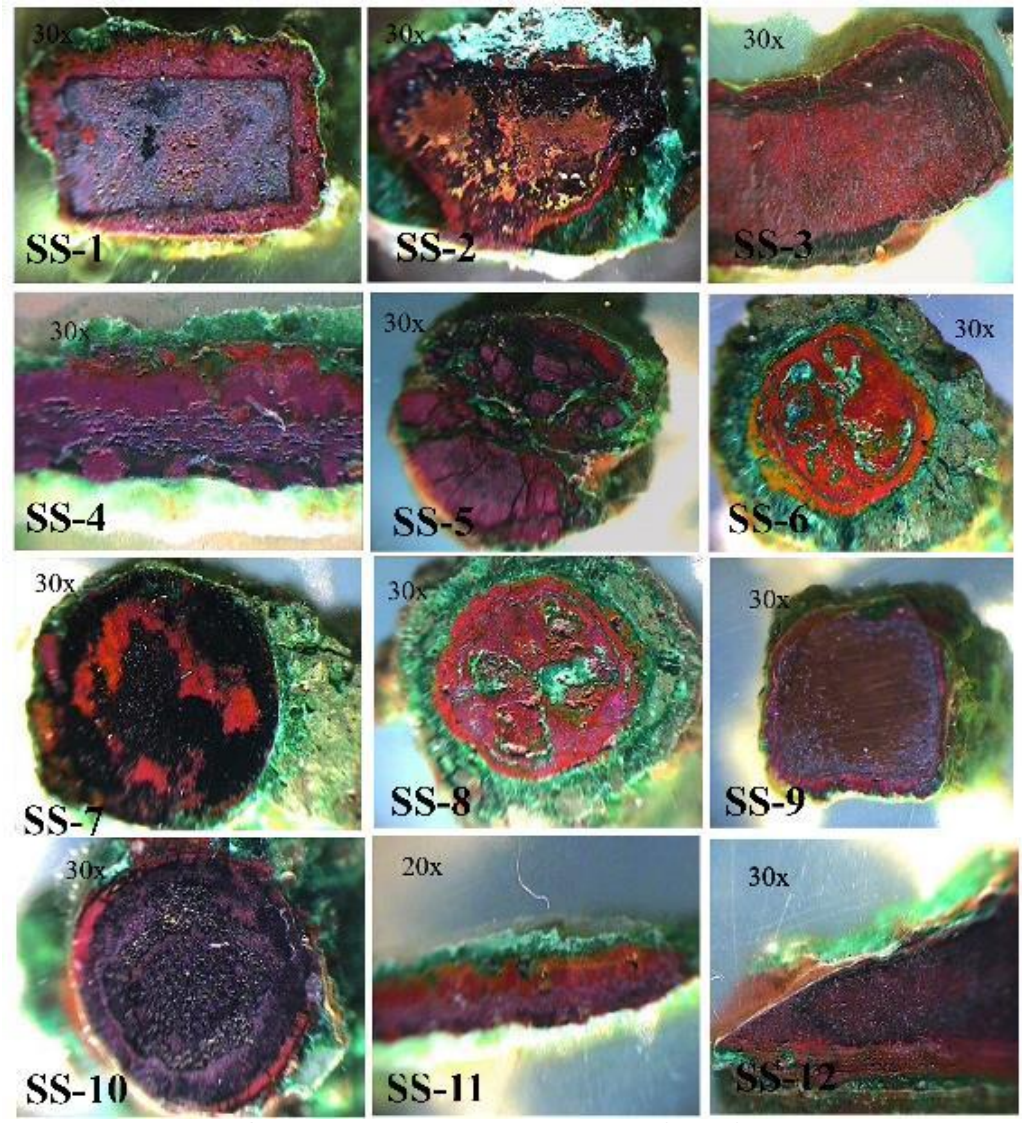

Figure 3: Cross-sectional stereo-microscopic images of *Shahr-i Sokhta* samples.

Table 3: Results of XRF analysis from the residential area and *Shahr-i Sokhta* cemetery section.

Sample	SiO_2	CaO	Al_2O_3	Fe_2O_3	MgO	K_2O	Na_2O	SO_3	CuO	TiO_2	P_2O_5	MnO	SrO	ZnO	Cl	V	L.O.I
SS-Ms1	43.50	14.94	13.14	2.95	4.57	2.00	0.87	0.38	0.05	0.78	0.15	0.13	0.32	-	0.02	0.01	**16.18**
SS-Ms2	39.35	15.11	14.85	3.01	3.36	1.18	1.60	0.18	0.03	0.73	0.13	0.13	0.34	-	-	0.01	**19.90**
SS-Go1	46.47	10.80	11.03	2.45	5.74	2.57	2.20	0.36	1.1	0.72	3.15	0.13	0.33	-	0.08	0.00	**12.87**
SS-Go2	50.41	13.74	13.13	0.43	4.70	1.77	0.81	0.53	0.80	0.40	2.13	0.11	0.29	-	-	-	**10.75**
SS-Go3	44.38	15.20	11.50	3.60	3.81	3.16	1/20	0.22	1.50	0.52	1.08	0.20	0.14	-	0.07	-	**13.42**

III.2. X-ray Fluorescence Studies for Characterizing the Soil

According to the XRF analyses obtained from the soil (Table 3) of the residential area SS-Ma1 and SS-Ma2, the percentage of compounds is the same, and only the amount of CaO and Fe_2O_3 is slightly higher than that of SS-Ma1. In the results of the XRF analysis of the soil of the residential area SS-Ma1, SS-Ma2, the highest amount is related to SiO_2, Al_2O_3, CaO and MgO, K_2O, Na_2O. TiO_2, and it is almost similar to the cemetery samples SS-Go1, SS-Go2. The composition of the cemetery soil is also similar to the residential part, and the amount of $SO_3 < 0.40\%$ was detected.

III.3. Synchrotron X-Ray Diffraction for Characterizing the Crystalline Phases

XRD analysis of four soil samples identified quartz, calcite, albite, muscovite, cuprite, gypsum and clinochloro minerals. Calcite is the most stable carbonate mineral, and the source of its formation is plagioclase, which contains calcium. In addition to these minerals, anorthite from plagioclase feldspar minerals, e.g., chamosite from silicate minerals, and sanidine from important potassium feldspar minerals have been identified in the soil of this area (Moazzez Lesko and Sharifiyan Attar, 2002; Abdellatief et al., 2022). In general, based on the results of XRD and XRF analysis, it can be said that the soil of this area is alkaline, and its constituent minerals in the residential and cemetery areas include silicates, carbonates, and sulphates. These minerals completely enclose metal objects.

Considering the amount of arsenic to copper in the corrosion layers of *Shahr-i Sokhta* alloys, no particular order in the migration of arsenic in the layers is seen. Therefore, the heterogeneity of these alloys in the distribution of arsenic phase and the imbalance in the phases caused by the post-deposition processes increase the complexity of corrosion (Budd and Ottaway, 1991). The first possibility, according to the amount of 12 to 18% of calcium oxide obtained from the XRF results, is due to the reaction of cuprous chloride with carbonate, which eventually leads to the formation of tenorite (Scott, 2002). The second possibility is that tenorite can be formed in different environments at high temperature, oxidation, and pH, and is expected as a stable phase with increasing pH between 8 and 14. Another possibility, according to the remains of burnt works in the *Shahr-i Sokhta*, is the formation of tenorite due to heat. Among other corrosion products, copper trihydroxy chlorides, including atacamite and paratacamite, were identified in the research works. Paratacamite has the highest strength of hydrogen bonding among other copper chloride products and is the most thermodynamically stable phase (Scott, 2002). According to the reactions (1-3), the products of bronze disease are considered. Clinoatacamite can be composed of atacamite, paratacamite, and gypsum, which is identified in most samples. Nantokite is an effective mineral in bronze disease, which, in the presence of copper chloride, easily turns into cuprite, copper oxide, and copper-based salts. The density and compression of the cuprite layer are probably important factors in preventing the complete oxidation of copper chloride (nantokite). In the progression of bronze disease, nantokite undergoes hydrolysis, leading to the formation of cuprous oxide as an intermediate corrosion product. The main reaction governing this process can be represented as follows:

(1) $2CuCl + H_2O \rightarrow 2HCl + Cu_2O$

According to the equation below, hydrochloric acid creates more nantokite according to the following reaction.

(2) $2HCl + 2Cu \rightarrow 2CuCl + H_2$

In the presence of sufficient oxygen and moisture, the following reaction is carried out with a free energy of formation of 1510 kJ mol^{-1}, which produces trihydroxy chloride.

(3) $4CuCl + O_2 + 4H_2O \rightarrow 2Cu_2(OH)_3Cl + 2H^+ + 2Cl^-$

According to the above reaction equation, chlorine can re-enter the reaction cycle and continue this cycle. Atacamite and paratacamite were identified in all the excavated objects, and these products are mostly uniformly located on the surface of the works. Due to the placement of the samples next to the bones of the

cemetery, hydroxyapatite (HA) with the formula $Ca_5(OH)(PO_4)_3$ is one of the most important compounds of bones and teeth, with a hardness of 5 Mohs, and constitutes about 70% of the structure of these minerals. The presence of this mineral in the sample is not far-fetched due to its location next to the bones. Another product is sinnerite, the combination of this type of structure with the formula $Cu_6As_4S_9$. It has a triclinic structure with a black to silver metallic color and a twin needle shape, with space group p1. Another corrosion product of chloroapatite was identified in samples SS-2 and SS-5 with the formula $Ca_5(PO_4)3Cl$, which possibly occurred due to the proximity of these objects next to the bone. The detection of chloroapatite supports the interpretation that the metal objects were buried close to human or animal remains, reinforcing archaeological stratigraphy or spatial analysis. The discovery of chloroapatite on metal samples SS-2 and SS-5 indicates a close association with bone material in the burial context, offering insights into the depositional environment, corrosion mechanisms, and taphonomic processes affecting archaeological metals. The detection of calcium arsenite (Ca_3As_2) in samples SS-2 and SS-3 (Fig. 4) and the presence of potassium vanadium arsenate hydrate in SS-6 indicate a complex pattern of chemical transformations during corrosion.

These compounds reflect both the original alloy composition and the specific environmental conditions to which the artifacts were exposed. In particular, the identification of silver arsenic selenide ($Ag_2As_2Se_3$) in SS-6 (Fig. 4) provides critical insight into the interactions among silver, arsenic, and selenium during corrosion processes. Such interactions suggest that trace elements present in the original alloy have contributed to the formation of secondary mineral phases, highlighting the intricate pathways of artifact degradation. From a metallurgical perspective, the presence of silver arsenic selenide may also shed light on the original composition of the alloy. Silver and arsenic could have been intentionally incorporated for functional reasons, such as improving hardness, ductility, or casting behavior, or they may reflect the use of locally available ores with naturally occurring trace elements. Selenium, though less commonly reported in ancient alloys, may have been present either as a natural contaminant or as part of early experimental alloying practices. These observations can provide clues regarding technological choices, including artisans' knowledge of alloy properties and their experimental approaches to combining metals. Moreover, such compositional insights have broader cultural implications. The deliberate or incidental inclusion of elements such as arsenic, vanadium, and selenium may indicate resource availability, trade networks, or even symbolic or ritualistic uses of certain metals. For instance, silver-bearing alloys could have been associated with prestige or specific cultural practices, and the choice of alloying elements may reflect local preferences or technological traditions that evolved independently of broader trade patterns. Archaeologically, the identification of these corrosion products is significant because it enables reconstruction of the original material composition, providing a clearer picture of the metallurgical knowledge and cultural context of the site. Additionally, understanding which secondary mineral phases formed under the prevailing burial or environmental conditions allows researchers to infer site formation processes and the long-term stability of different alloy components.

Overall, these findings underscore the value of detailed microanalytical studies in bridging metallurgical science and archaeological interpretation, offering insights into both the technological and cultural dimensions of ancient metal production and use. Another corrosion product identified in SS-6 is copper sulfide with the formula Cu_xS_y, which can indicate the presence of Cu_2S chalcocite or CuS Covellite impurity in the corrosion products. Sulfide originates from the reduction of sulfates by bacteria (SRB). Also, the biosorption of As (III) and As (IV) on sulfate-reducing bacteria leads to the removal of significant amounts of arsenic (Panagiotaras et al., 2015).

III.4. Micro-chemistry of the metals by SEM-EDX

Among the objects excavated from this area, only two samples had uncorroded metal cores. The SEM-EDX analysis conducted to investigate the corrosion behavior and chemical composition of the artifacts revealed that sample SS-3, originating from the residential area, contains approximately 91% copper, while sample SS-10, from the cemetery sector, contains approximately 93% copper (Table 4). In both samples, the presence of oxygen on the surface indicates partial surface oxidation, which is consistent with the formation of corrosion products such as cuprite (Cu_2O) or other copper oxides. The slightly higher copper content in SS-10 suggests potential differences in the original alloy composition or the extent of corrosion processes between the residential and cemetery artifacts. Overall, these findings provide insight into the preservation state of the artifacts and indicate that while the bulk metal remains largely unaltered, surface oxidation reflects environmental interactions over time, which may inform both conservation strategies and the understanding of metallurgical practices at the site.

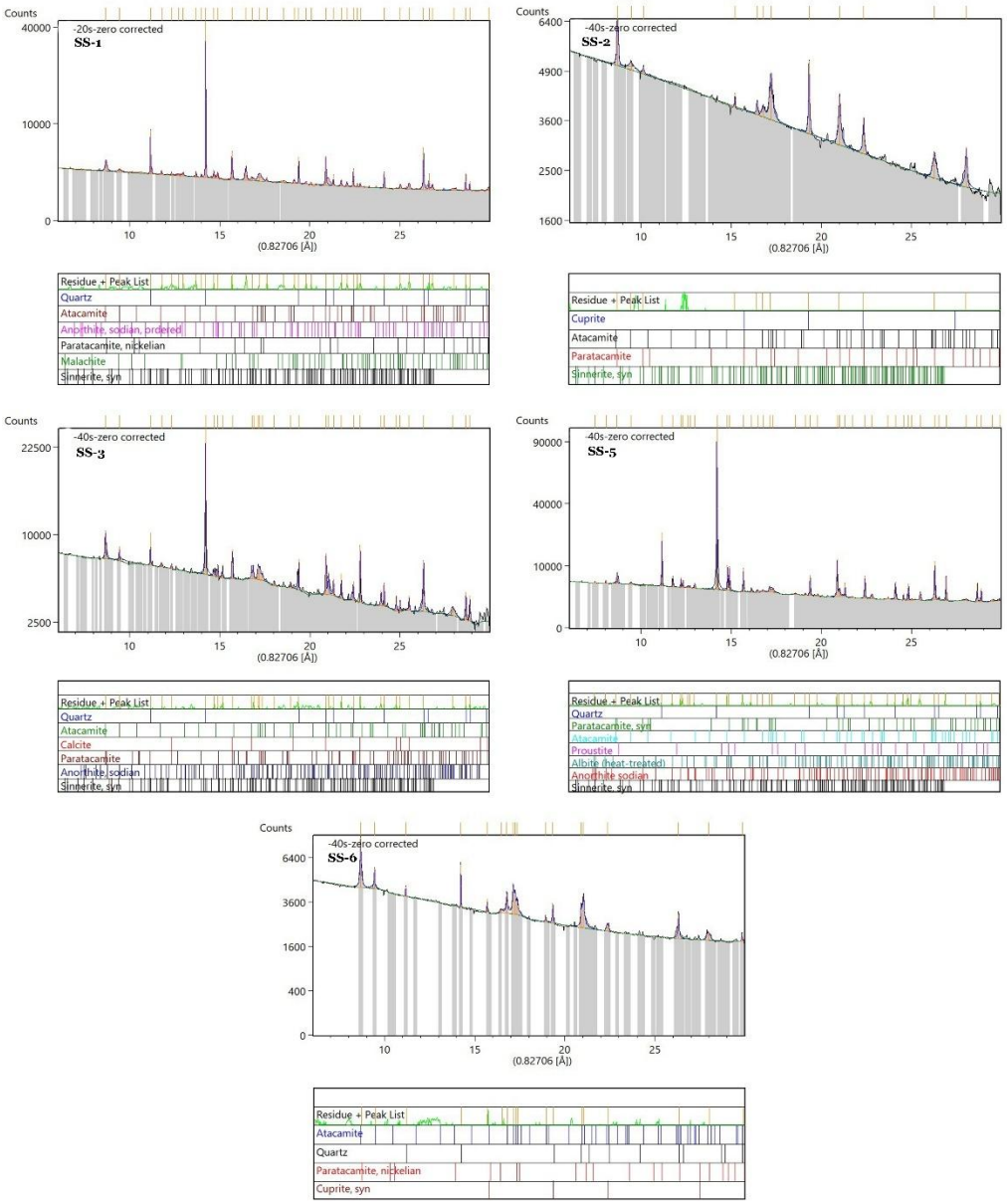

Figure 4: Synchrotron-based XRD diffractograms of the black corrosion products of some investigated samples.

Table 4: EDX analysis of the chemical composition of elements in the alloys from residential (SS-3) and cemetery (SS-10) of *Shahr-i Sokhta* (Wt.%).

Sample	O	Cu	As	S	Fe	Sn	pb	Zn
SS-3	3.84	90.79	0.36	1.66	1.49	0.86	0.24	-
SS-10	2.50	92.81	0.49	1.41	2.28	0.51	0.30	-

According to the SEM-EDX analysis, the percentage of arsenic in the *Shahr-i Sokhta* objects in the equilibrium diagram (Cu-As) is marked with a red area in Figure 4. Regarding the phase diagram in casting conditions, α (Cu, As) is formed during the solidification of arsenical copper, in the solid solution state (Fig. 5). The amount of arsenic in the sample SS-10 is 0.5w% and it reaches in the sample SS-3 of about 0.36w%. The amount of iron (occurred by the co-smelting process of iron-rich ores) in these two samples is 1.5 to 2.30w% and the amount of tin is 0.51 to 0.90w%. Sulfur is approximately between 1.5w% and 1.7w%. Lead is around 0.51w% and goes up 0.86w%. These percentages has high variation as shown in similar (Rehren, 2003; Dardeniz 2020).

Microanalysis of some objects have proved that the *Shahr-i Sokhta* alloy contains Cu-As-Sn compounds, however, the obtained data indicated the low amount of arsenic in this alloy (Fig 6, Table. 5). The identification of the α(Cu, As) solid solution phase not only

corroborates earlier reports but also provides more precise information regarding the phase composition and arsenic content, which was quantitatively determined. In alloy type. Our results indicate that, in addition to arsenic, tin is present in quantities consistent with an As–Cu–Sn bronze (Radivojević et al., 2013; Thornton and Roberts, 2009).

While the arsenic content could have been reduced during manufacturing, firing, and subsequent corrosion, the most plausible pathway for obtaining such tin levels is smelting from ores containing both tin and arsenic (Weeks, 2012). Based on EDS analysis, sample SS9 represents the corrosion product of an alloy fundamentally different from the others, with an inherently high arsenic content and the absence of sulphur, yet with consistent carbon detection. In contrast, the other analyzed samples have lower arsenic content, contain tin and lead, and exhibit sulphur but no detectable carbon. These compositional differences suggest the use of distinct alloys and potentially different ore sources, possibly fahlores containing both tin and arsenic (Pernicka, 2014).

This differentiation is significant for understanding whether the use of arsenical copper was intentional or incidental. When viewed alongside regional archaeometallurgical data, the SS9 composition, combined with the others, appears to bridge a technological phase between the late arsenical copper tradition and the early adoption of tin bronze in the region (Radivojević et al., 2013). Thus, although the qualitative trend agrees with previous studies, our results provide new quantitative data on elemental composition, phase identification, and technological choice, contributing to a more nuanced reconstruction of early metallurgical practices.

The presence of α(Cu, As) indicates that the artifacts were subjected to a process of refinement and cooling within solid solution fields, a process that has been demonstrated to influence their mechanical properties, as evidenced by an enhancement in hardness and strength when compared to pure copper. The results of the SEM-EDX and metallographic analyses indicate that the levels of arsenic are generally low, thereby suggesting the phenomenon of unintentional alloying. This is perhaps attributable to the smelting of naturally arsenic-bearing copper ores (e.g., fahlores), which is a subject of interest in this study. Arsenical copper, an alloy of copper and arsenic, was widely employed in the Chalcolithic and Early Bronze Age due to its enhanced hardness and favorable casting properties (Lechtman and Klein, 1996). This technological choice reflects a metallurgical stage preceding the widespread adoption of tin bronze, which became standard in the Near East around 3000 BCE (Craddock, 1988). The transition to tin bronze was influenced by the alloy's superior casting quality, ductility, and corrosion resistance, despite tin being relatively rare and difficult to obtain in the ancient world (Thornton and Lamberg-Karlovsky, 2004).

Moreover, the use of arsenical copper may indicate local metallurgical traditions that developed independently of early tin trade networks. Evidence from sites on the Iranian plateau, such as Tepe Yahya, shows that native arsenical copper and copper-arsenide ores were smelted to produce functional bronze objects (Beale, 1973). This suggests that metallurgists experimented with arsenic as an alloying element either because of local resource availability, technological preference, or as part of early alloying experimentation.

III.5. Metallography and Optical Microscopy

Investigations showed that the samples still preserved their metal core, while surrounded by gray-colored reaction products and corrosion structures. In the SS-3, SS-4, and SS-6 samples, the presence of severe corrosion products is well-defined from the edges of the main surface into the inside. To identify the manufacturing method, the samples were etched using an alcoholic solution of iron (III) chloride (Scott,1991). In the SS-10 sample, the twins in the structure indicate that the work underwent heat treatment (annealing) to increase its malleability (Kopezky et al., 1985). Within the microstructure of the SS-3, SS-4, and SS-6 samples, the presence of impure slag can be seen in Figure 7A. The chemical composition of the metallic objects and slag provides information about the sources of metals and the chemical composition of the bronze objects.

The chemical composition of the metal in a workshop is varied, of course, because the ores, furnaces, crucibles, and variables of temperatures all alter the chemical composition of the metallic items. (Keykhaeia et al., 2012). The micro-texture of the SS-3 sample from Shahr-i Sokhta before etching has shown on the left side and after etching on the right side (Fig. 7B). Due to the microscopic observations, some sulphide impurities and lead globules are scattered (Fig. 7C, D). The presence of copper oxide in the form of globules in this image could have occurred due to the corrosion actions that had been selectively attacked through the burial of bronze objects (Scott, 1991).

This structure, which is considered the dominant structure in ancient casting, grew in the form of a leaf until they stretched each other (Fig. 7C, D). Such a structure is frequently caused by the higher percentage of impurity within the metal or alloy as a type of segregation that occurs during the casting process (Scott, 1991). From an archaeological perspective, it provides evidence of ancient metallurgical processes, especially those characterized by low-purity inputs, non-homogeneous alloys, and corrosion-induced transformations. The technological level, the availability of resources, and post-depositional changes affecting the artifacts are all critical factors in reconstructing

ancient societies and their craft traditions. The presence of dendritic arms can include coring dendrites that occur during the solidification of a copper alloy (Philip et al., 2003). Therefore, increasing cold work lowers the recrystallization temperature (Dungworth, 2013). In the SS-10 twin lines, a large accumulation of strain lines has been identified (Fig.7E, F). Consequently, the presence of intergranular corrosion in the corroded parts and holes caused by gas leakage has also been determined (Fig. 7G).

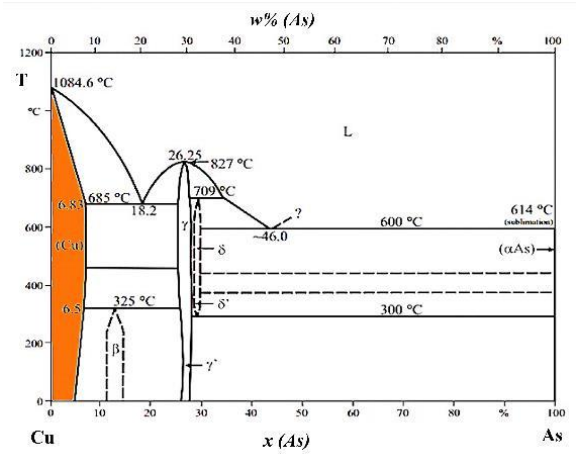

Figure 5: Phase diagram (Cu-As), the red area shows the amount of arsenic in *Shahr-i Sokhta* objects.

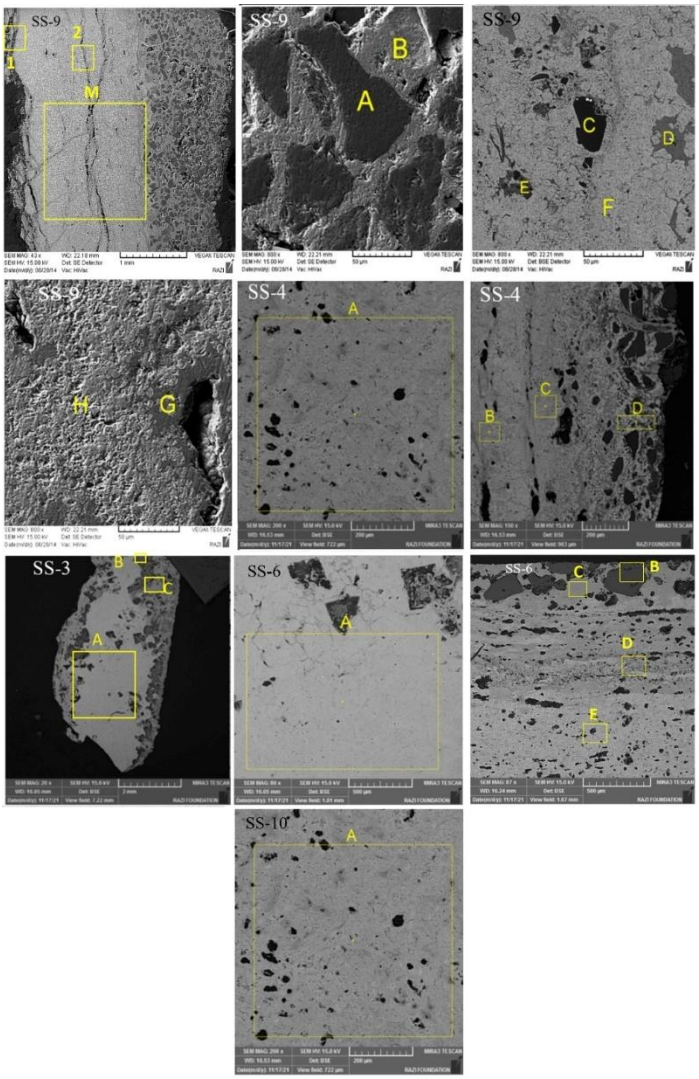

Figure 6: SEM images of the samples SS-3, SS-4 and SS-9 which all areas of interest for determining the microchemistry of the objects (alloy).

Table 5: SEM-EDX elemental analysis related to copper alloys (Cu-As, Sn) of *Shahr-i Sokhta*.

Sample	O	Si	Cu	As	Cl	Sn	S	Ca	K	C	Mg	Ag	Al	Fe	Pb
SS-9-1	7.01	0.57	79.33	8.66	0.48	-	1.60	-	-	1.17	-	-	-	-	-
SS-9-2	21.9	9.00	39.40	12.13	0.81	-	-	-	0.91	1.97	-	-	4.98	3.60	-
SS-9-M	13.36	6.49	70.48	3.56	4.46	-	-	-	0.65	5.44	-	-	-	-	-
SS-9-A	17.87	18.72	25.94	-	9.00	-	-	2.42	0.64	9.54	0.02	-	6.58	0.54	-
SS-9-B	17.87	0.68	64.20	-	14.26	-	-	-	-	1.33	0.96	-	-	-	-
SS-9-C	49.69	48.35	-	-	-	-	-	-	-	1.97	-	-	-	-	-
SS-9-D	13.36	0.33	61.42	-	15.84	-	-	1.52	-	1.40	3.9	2.06	-	-	-
SS-9-E	6.45	0.17	91.29	-	1.17	-	-	-	-	0.57	0.19	-	0.16	-	-
SS-9-F	7.09	0.33	88.76	1.80	-	-	-	0.86	-	1.10	-	-	-	-	-
SS-9-G	11.98	-	60.83	16.58	5.96	-	-	4.65	-	-	-	-	-	-	-
SS-9-H	8.95	-	86.86	2.25	-	-	-	-	1.14	0.81	-	-	-	-	-
SS-4-A	23.03	-	68.82	2.39	1.85	1.27	0.60	-	-	-	-	-	-	-	**2.04**
SS-4-B	21.79	-	72.99	0.59	2.88	0.31	0.34	0.60	-	-	-	-	-	-	**1.09**
SS-4-C	24.04	0.18	71.97	0.24	2.58	0.38	0.00	0.00	-	-	-	-	-	-	**0.60**
SS-4-D	27.75	1.69	63.17	1.34	2.10	0.85	-	0.10	-	-	-	-	0.63	-	**1.08**
SS-3-A	4.84	-	90.79	0.36	-	0.89	1.66	-	-	-	-	-	-	1.49	-
SS-3-B	12.4	-	83.92	1.03	0.31	0.94	0.03	-	-	-	-	-	-	083	**0.54**
SS-3-C	14.3	-	80.84	0.23	2.3	0.03	0.21	-	-	-	-	-	-	1.61	**0.48**
SS-6-A	22.49	-	72.97	0.27	2.93	0.54	0.00	-	-	-	-	-	-	-	**0.80**
SS-6-B	36.85	50.01	2.5	0.24	0.00	0.21	0.21	4.29	1.57					0.5	**063**
SS-6-C	9.81	0.00	84.97	3.4	1.02	0.21	0.23								**0.36**
SS-6-D	5.2	-	76.39	16.3	0.91	0.5	0.28								**0.42**
SS-6-E	4.5	-	90.1	0.23	3.4	0.56	0.38								**0.83**
SS-10A	2.5	-	92.81	0.49		0.51	1.41							2.28	**0.03**

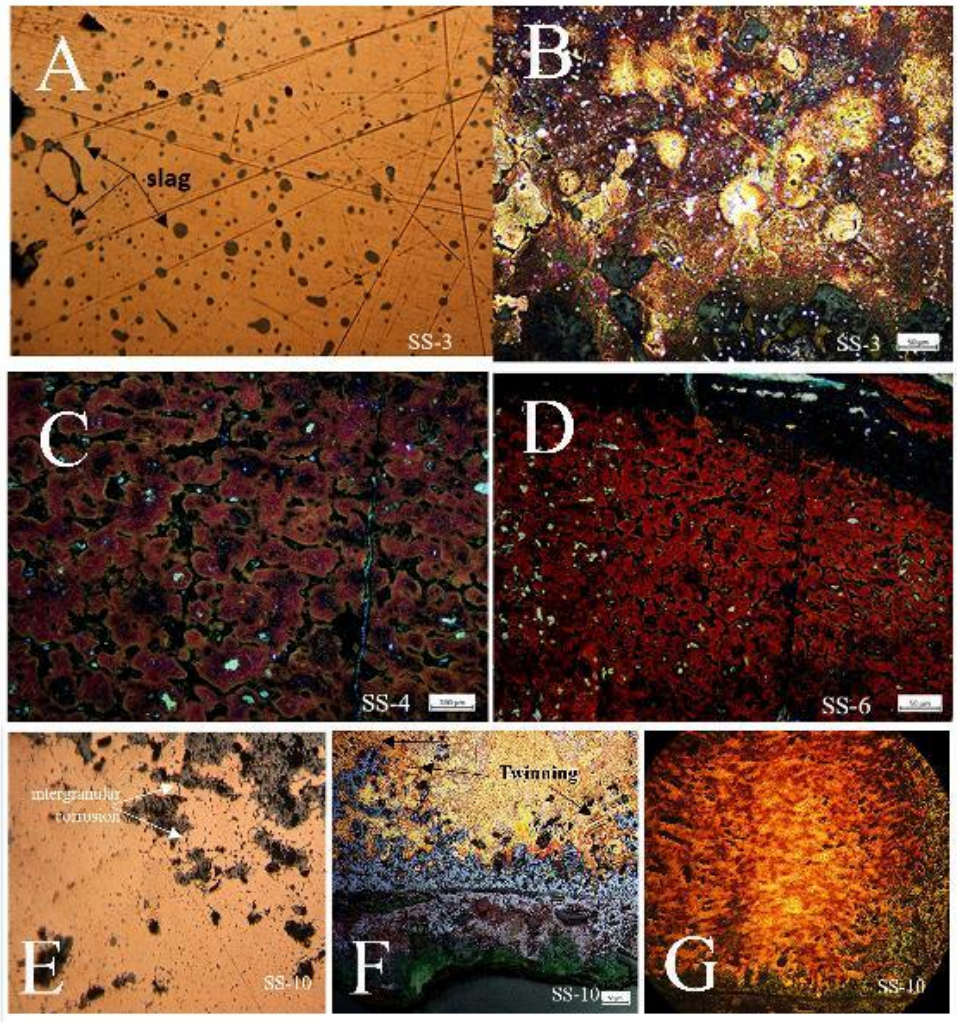

Figure 7: The metallographic images of SS-3, SS-4, SS-6 and SS-10 samples before and after etching.

IV. Discussion

IV.1. Black patina or corrosion

Most of the samples have black corrosion that started from the surface of the objects and penetrated to the depth of the work. According to the XRD analysis, the corrosion of the Surmedani (kohl container rod) consists of tenorite (Fig. 8A, sample SS-1). This corrosion product, which is found next to and on the surface of cuprite, is usually found in burial environments, under heat, although tenorite has a stable range in the Pourbaix diagram, but it is rarely seen in practice (Scott, 2002). Tempering occurs when an object is slowly heated in air. Oxidation of most copper compounds in air eventually produces tenorite when heated. On the other hand, tenorite may be created in the presence of moisture and air (Scott, 2002). Azurite and malachite can turn into tenorite along with calcite, $CaCO_3$, or calcium oxide, CaO. The presence of calcium compounds, by creating a high local pH, can be a favorable condition for the formation of tenorite. However, by Eh=0.8 and at pH between 8-14, tenorite might have been expected as the stable phase instead of malachite or azurite. Another weak possibility is that the black areas formed by copper hydroxide in the cathodic regions of local cells are precipitated by the electrolytic activity of the salty environment (Fig. 8B, sample SS-8).

The structure of internal corrosion in the form of internal black strips of tenorite placed below the main surface, and red corrosion products (cuprite) can be seen in some parts. In the outer part of the corrosion, the red layers of cuprite are surrounded by green layers, on which there are sediments from the burial environment. The observed corrosion layering tenorite beneath cuprite and green surface deposits reflects complex stratified corrosion processes influenced by soil chemistry and environmental fluctuations.

These findings enhance our understanding of ancient material preservation, site-specific taphonomic processes, and contribute to the broader reconstruction of the depositional and chemical history surrounding archaeological copper-based artifacts. In the field of archaeometallurgy, taphonomy plays a pivotal role in facilitating the discernment of original features that are intrinsic to the manufacturing process from those that have undergone post-depositional alterations. The analysis of corrosion layers is instrumental in the reconstruction of burial environments. The comprehension of the preservation state and the object's history is paramount. The recognition of alterations in alloy composition, resulting from leaching or oxidation, is crucial.

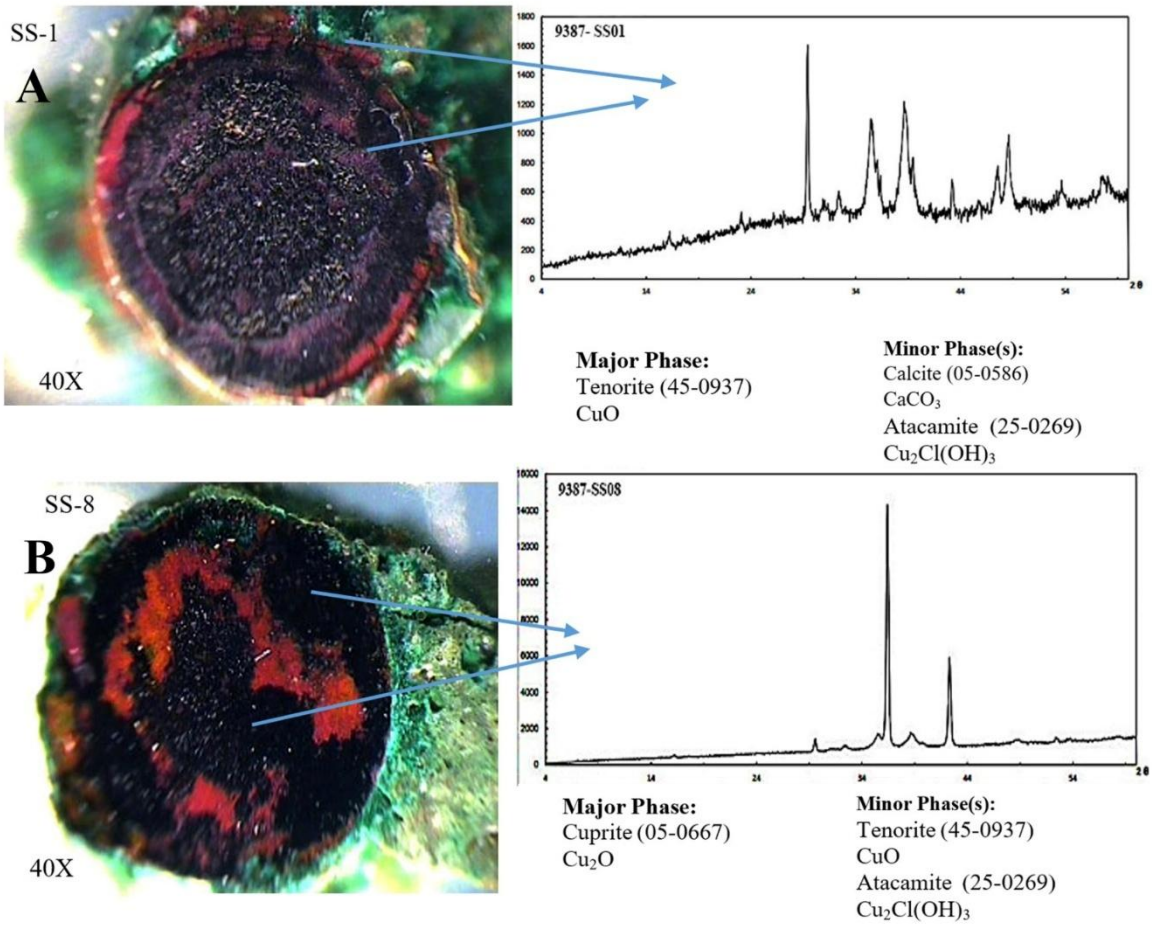

Figure 8: A: XRD analysis of black corrosion products in sample SS-1, B: in sample SS-8.

The distribution map of the elemental constituent is given in Figure 9 from the sample SS-6. Elemental mapping shows that oxygen is concentrated on the surface of the objects in accusation with quartz and aluminum on the surface, which are strongly attached to the corrosion products and related to the burial environment of the effect. The concentration of arsenic can be seen on the surface and in the middle of the sample in the form of a strip in the background. Sulfur and lead elements are uniformly distributed in the field. There is no correlation with the chlorine element, and the concentration of chlorine is lower in the inner parts. In the outer regions of the corrosion layers, distinct stratification is observed, consisting of red strips of cuprite (Cu_2O) interspersed with narrow green layers of arsenic corrosion products.

These layers are further surrounded by green chloride corrosion products, upon which additional deposits and sediments have accumulated. The original surface of this artifact was not recognizable due to changes caused by the burial environment and the progressive rate of corrosion. Within the central portion of this corrosion structure, black tenorite (CuO) is present, often accompanied by cracks and micro-cracks that are partially filled with green arsenic-derived products. This complex, multilayered morphology reflects a combination of environmental exposure, localized chemical interactions, and the heterogeneous progression of corrosion over time. These findings enhance archaeological interpretations by revealing the material history, burial conditions, and metallurgical choices associated with the artifact.

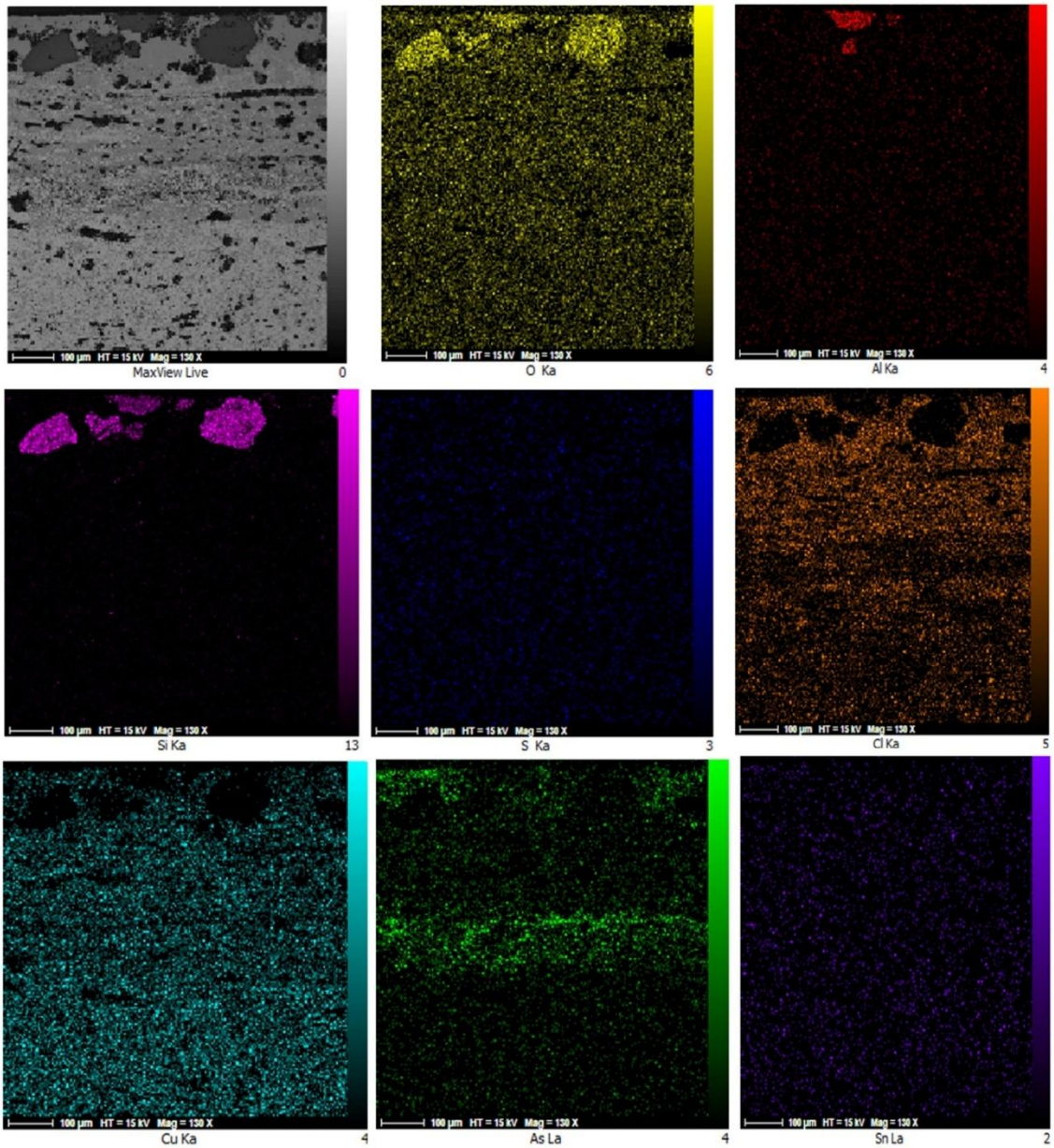

Figure 9: Image analysis of constituent elements map from sample SS-9, *Shahr-i Sokhta.*

This type of corrosion has been separated from the original surface of the sample. This can be identified through occurrences of red corrosion of cuprite, covered by the green corrosion products of copper chloride, such as atacamite and paratacamite, and tenorite is also seen in some parts (Fig. 10A, B). According to the polarized images, another one of these corrosions is band-shaped corrosion that can be seen in the patina morphology and layering of most ancient bronzes and has a sandwich structure and is characteristic of the Liesegang phenomenon (Fig. 10C), where the primary patina layers are placed on top of each other or slightly overlapped with each other. Secondary patina can be mentioned as mixed layers of corrosion products that occur during chemical processes in heterogeneous liquid-solid systems and the successive formation of the products of Liesegang rings (Fig. 10D).

Patinas include cuprite and tenorite, copper sulfides and copper arsenates are formed by overlapping or alternating with atacamite, paratacamite layers. These findings reflect the use of arsenical copper, the influence of microbial and chloride-rich environments, and sequential burial phases. They offer valuable information for reconstructing alloy compositions, understanding burial site chemistry, and guiding conservation efforts for ancient copper-based artifacts. Copper chlorides and copper hydroxy sulfates, and environmental deposits such as gypsum, silicate, soils, and other metal mineralization have led to the separation of infiltration and diffusion processes in the lower layers.

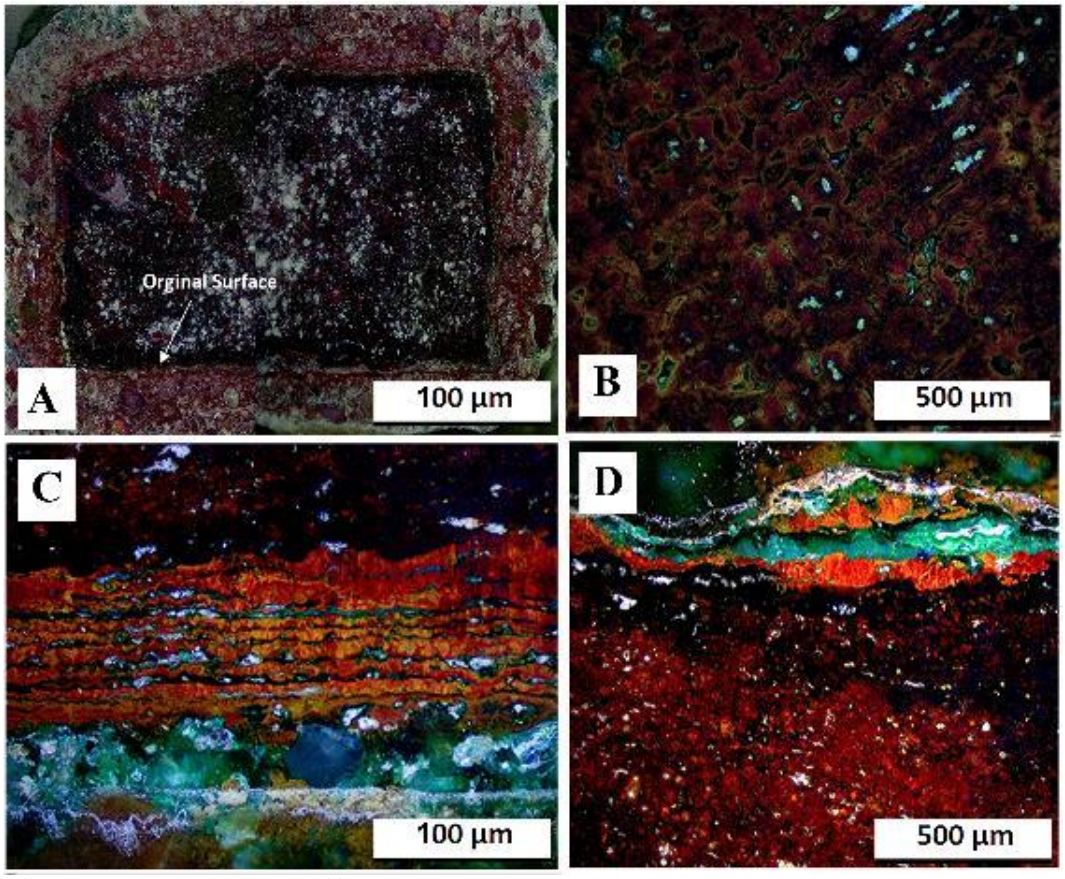

Figure 10: A: Microscopic images of sample SS-6, which contains various corrosion products, including cuprite, tenorite, and trihydroxy chloride corrosion products. B: SS-4 in the dark background and well-defined dendritic structure, which characterizes the casting method. The presence of blue grains indicates copper arsenide. C: SS-8, numerous smaller or secondary bands which were formed as Liesegang rings. D; SS-9, parting of penetration and diffusion processes within the corrosion layers.

IV.2. Stratigraphic Investigation on the corrosion morphology

According to microscopic observations and SEM-EDX analyses, three morphological structures of corrosion were identified in the arsenical copper artifacts of *Shahr-i Sokhta*. The morphological structure of the first group has two parts. It includes the outer part and the inner part (Fig. 11). In corrosion studies of metallic artifacts, the *original surface* marks the boundary between the metallic core and outer corrosion layers. Outer parts, above this surface, are in contact with the burial environment and include green chloridic layers, arsenic-bearing products, cuprite, and mineral deposits, usually brittle and porous.

Inner parts, below the surface, contain dark red, orange, yellow, or black corrosion (e.g., tenorite), often cracked and filled with green arsenic-bearing products. The outer part consists of two layers, which contain

green corrosion covered with buried hardened sediments, and the inner part is placed on the main surface and has dark red products to yellow and orange tones. The inner part is also divided into two layers, which are related to the metal core of the alloy. The interface between the red corrosion, between the outer part and the inner part, is the main surface. The black corrosion is located below the main surface, and the corrosion grows from the main surface without changing the volume or specific resistance towards the alloy (Robbiola et al., 1998).

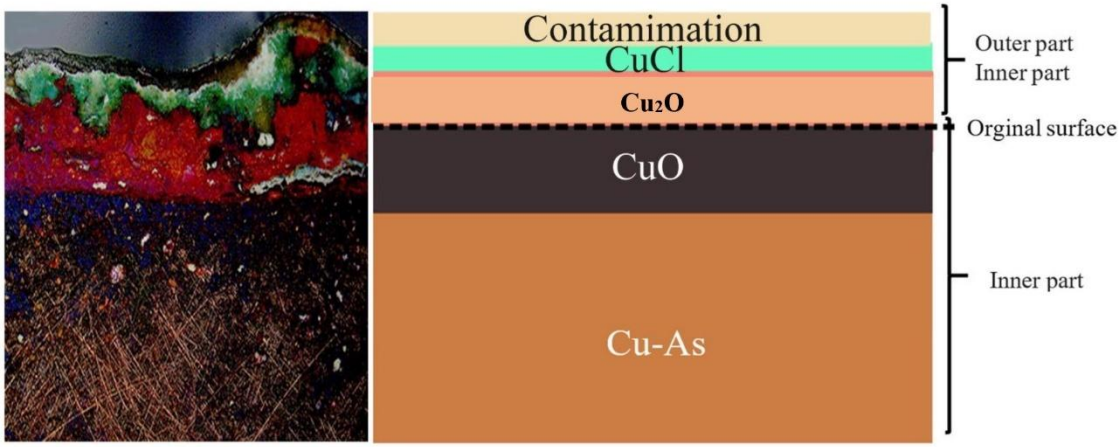

Figure 11: The schematic diagram of the corrosion morphology of the works obtained from the area of the *Shahr-i Sokhta* has two parts, including the outer part and the inner part. The outer part consists of green corrosion covered with hardened buried sediments. The inner part is related to the metal core of the alloy, and is defined as a separation between the red and black layers.

In the morphological structure of the second group, three layers of corrosion have been seen in the arsenic copper alloy of *Shahr-i Sokhta*, which has completely turned into corrosion products, and due unclarity of the main surface is not clear (Fig. 12). The outer layer has bright green corrosion products, which include copper trihydroxy chloride compounds. Minerals are very bulky and hard in some parts, and thin in others. The middle layer, which contains corrosion products in red, and sometimes this layer is repeated on top of each other in the form of thin strips with bright red color tones. The black internal corrosion layer is located under the cuprite layer, which is powdery in the center and harder in the middle corrosion layer. In this type of corrosion morphology, the presence of black corrosion products has penetrated the outer and middle parts, and in some cracks and corrosion fractures, it has been seen scattered in all three layers.

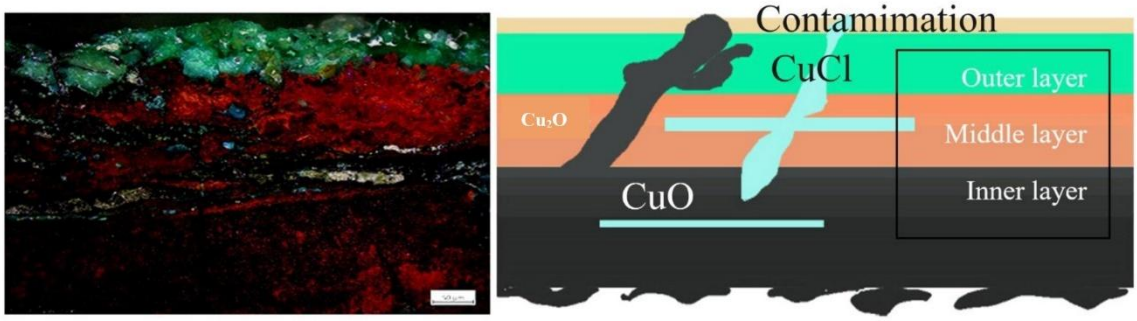

Figure 12: Schematic diagram of the corrosion morphology of the second group of *Shahr-i Sokhta*, which includes the outer layers consisting of copper chloride, the middle layer consisting of cuprite, and the inner layer consisting of tenorite.

In the morphological structure of the third group in the arsenical copper alloy of *Shahr-i Sokhta*, there are parts of copper trihydroxy chlorides in the form of accumulation in the outer layer of corrosion. In the middle parts, the red cuprite layer has irregular holes filled with arsenic. In the inner layer, which has completely turned into tenorite, there are stretched veins full of arsenic compounds, which were eventually caused by the loss of this part due to the incoherent structure of tenorite. These findings confirm the use of arsenical copper metallurgy and illustrate how environmental conditions led to the complete mineralization and structural failure of the artifacts. The loss of original surfaces underscores the importance of archaeometric methods in reconstructing technological and cultural information from highly degraded materials.

IV.3. Corrosion Mechanism

The corrosion mechanism in the arsenical copper artifacts from the *Shahr-i Sokhta* site primarily involves the spontaneous degradation of the base alloy alongside

the formation of various surface corrosion products (Robbiola et al., 1998). Based on the burial environment and artifact contexts, the primary deterioration appears to occur within internal corrosion zones, where electrochemical transformations are especially active. One of the initial steps in corrosion under burial conditions involves the reaction of metallic copper with environmental agents such as moisture, oxygen, and chloride salts. These interactions result in the formation of copper chloride compounds, which are unstable and readily convert to other species in the presence of alkaline conditions.

A key intermediate formed during this process is spertiniite ($Cu(OH)_2$), a blue-colored, amorphous copper hydroxide. Although spertiniite is rarely stable as a long-term corrosion product, it serves as a transitional phase, often transforming into other compounds such as atacamite, particularly when subjected to drying in alkaline environments (Chhabra and Chhabra, 2021).

In copper and copper-based alloys, chloride ions in an alkaline setting are particularly aggressive, promoting the breakdown of protective surface layers and initiating localized pitting corrosion (Scott, 2002; Becerra et al., 1988). While hydroxide ions generally enhance passivation, they can also facilitate copper dissolution, forming layered structures composed of hydroxides and oxides. In such cases, divalent copper species play a dominant role in further corrosion and the buildup of surface films (King, 2002). This outer layer can, in some cases, offer partial passivation, reducing the corrosion rate (Schmutzler et al., 2017).

Simultaneously, arsenic present in the alloy undergoes oxidation and hydrolysis reactions. These processes lead to the formation of arsenate species, which may further interact with copper compounds and chloride ions in the burial environment. Under specific conditions, stable copper arsenate minerals can form. However, due to the strongly alkaline conditions at *Shahr-i Sokhta* (pH > 10), and high chloride concentrations, the formation of copper arsenates is less favored. Pourbaix diagrams suggest that, in these conditions, the dominant corrosion products are likely copper oxides such as cuprite (Cu_2O) and tenorite (CuO).

Thermodynamic analysis shows that arsenic oxides generally form more readily than copper oxides under similar conditions, due to their lower Gibbs free energy. The presence of chloride ions further exacerbates corrosion, as they facilitate the formation of copper(I) chloride (nantokite), which penetrates the corrosion layers and promotes pitting. In environments with limited water and oxygen, nantokite can remain relatively stable. However, in moist conditions, it gradually oxidizes to form copper(I) oxide (cuprite), contributing to the growth of protective but brittle layers. Deeper within the artifacts, the primary copper phase (Cuα) is subject to transformation into cuprous chloride. These regions can then evolve into copper trihydroxychloride minerals, especially in the presence of both oxygen and moisture. These transformations are thermodynamically favorable and proceed spontaneously under burial conditions.

The outer corrosion layers often exhibit products such as atacamite and paratacamite—two copper hydroxychloride minerals. Their formation results from the oxidation and hydrolysis of previously formed cuprous chloride. X-ray diffraction (XRD) analyses confirm the presence of these phases in corrosion products at *Shahr-i Sokhta*. Scanning electron microscopy (SEM-EDX) and polarizing microscopy observations indicate that these transformations are accompanied by internal stresses within the corrosion layer, causing cracking, delamination, and eventual fragmentation of the corrosion products (Scott, 2002).

Soil moisture levels strongly influence the corrosion behavior. Measurements from both the residential and cemetery areas of the site revealed that the residential area exhibits higher humidity (4–4.3%) compared to the cemetery (2.7–3.9%) (Azoor et al., 2019). These moisture differences have likely contributed to the spatial variation in corrosion intensity and mineral composition across the site. Although atacamite and paratacamite are typically associated with acidic environments, their presence in the alkaline soils of *Shahr-i Sokhta* (pH > 10) suggests either localized pH fluctuations or dynamic microenvironments within corrosion layers.

Tylecote (1979) emphasized the role of soil pH in determining long-term corrosion patterns, noting that acidic soils are generally more corrosive than alkaline ones. Nonetheless, the occurrence of these corrosion products might also reflect seasonal or microenvironmental changes that temporarily alter local pH values.

In some regions of the site, competitive reactions between copper hydroxychlorides and carbonate species such as malachite have occurred. These interactions, facilitated by the presence of carbon dioxide and sufficient oxygen, result in the transformation of corrosion layers into mixed copper carbonate-hydroxide phases. These complex pathways further illustrate the diverse and dynamic nature of post-burial alteration processes.

Overall, the observed variations in corrosion products and mechanisms across the *Shahr-i Sokhta* site reflect the influence of burial conditions such as moisture content, pH, and the presence of aggressive ions like chloride. These findings are valuable for reconstructing the taphonomic history of copper alloy artifacts and for developing more effective conservation strategies tailored to site-specific conditions.

V. Conclusion

Shahr-i Sokhta, one of the most significant Bronze Age sites in southeastern Iran, provides critical evidence for early metallurgical practices in the region. This study, focusing on the characterization of As-Cu alloys, aimed to gain deeper insight into the chemical composition, microstructure, and corrosion behavior of arsenical bronzes excavated from both the residential and cemetery areas of the site.

Moisture analysis of soil samples revealed higher humidity levels in the residential area compared to the cemetery, with measured values ranging from 3.5 wt% to wt 4.5%. XRF analysis showed a consistent composition of soil compounds across samples, with SO_3 content below wt 0.40%. XRD analysis identified quartz, calcite, albite, muscovite, cuprite, gypsum, and clinochlore minerals in four soil samples. Corrosion products detected through XRD include copper arsenates and copper trihydroxy chlorides, such as atacamite and paratacamite. Given the burial conditions of the site, the dominant corrosion phases are associated with arsenical copper, cuprite, and tenorite. The presence of sinnerite further suggests regeneration conditions within the burial environment. Considering the burial environment, soil chemistry, and stratigraphic distribution, the most likely primary formation pathway for tenorite is natural oxidation of copper carbonates under moist, high-pH conditions, with electrolytic micro-galvanic activity potentially contributing to localized internal development.

These corrosion products reflect complex interactions between the burial environment and the original alloy compositions. The identification of hydroxyapatite and chloroapatite, particularly in samples located adjacent to bone remains, supports a strong correlation with skeletal material, shedding light on site taphonomy and burial stratigraphy. Moreover, the detection of arsenic and selenium-bearing corrosion products such as silver arsenic selenide and calcium arsenite indicates the use of arsenic-rich alloys, as well as post-depositional chemical and microbial transformations. The identification of copper sulfides and the inferred activity of sulfate-reducing bacteria point to microbially influenced corrosion processes in anaerobic conditions.

Compositional analysis of the metal artifacts using EDS-SEM revealed the presence of Sn-As-Cu compounds; however, further investigations using polarized light microscopy and EDX-SEM confirmed only a low arsenic content and no evidence of tin. This suggests a reliance on arsenical copper, possibly derived from naturally arsenic-rich ores or through unintentional alloying. The presence of α(Cu, As) solid solution phases confirms this interpretation and places this site within the broader framework of metallurgical traditions in the eastern Iranian plateau during the Chalcolithic to early Bronze Age. Corrosion structure analysis categorized the deterioration into three primary groups. The third level of deterioration showed deterioration factors (Fdet) between 1.50 and 3.00. Average deterioration (Fdet) is rated on a scale from 1 (well preserved) to 5 (heavily corroded), indicating the extent of corrosion or damage to the object. Two main corrosion structures were identified. The first included an external section composed of two layers green corrosion and a layer of dark red to orange corrosion products and an internal section with a metal core and alternating red and black layers, where the red interface represents the original metal surface.

The three types of corrosion structures observed are:

(1) Internal corrosion characterized by black inner tannery bands around the original surface, with cuprite observed in certain areas and surrounded by red cuprite layers embedded in green corrosion;
(2) An external corrosion structure with cuprite layers accompanied by arsenic-rich bands;
(3) A corrosion morphology consisting of red cuprite layers covered with atacamite, paratacamite, and occasionally tenorite.

The presence of copper trihydroxy chlorides in these contexts points to competitive corrosion reactions among malachite, atacamite, and paratacamite, which may co-form in oxygen-rich burial environments. Overall, these findings offer a multifaceted understanding of the metallurgical choices, burial conditions, corrosion mechanisms, and post-depositional transformations that shaped the preservation of metal artifacts at *Shahr-i Sokhta*.

Acknowledgements

The corresponding author also expresses sincere appreciation to the SESAME Synchrotron Facility for the accepted and funded project ID201900116. The experiments were performed at ID09-MS/XPD beamline with the collaboration of the SESAME staff. The authors of this article wish to express their profound gratitude and appreciation to the President of Isfahan University of Arts for their invaluable support in establishing a conducive research environment for this project.

References

Abdellatief, M., Najdawi, M.A., Momani, Y., Aljamal, B., Abbadi, A., Harfouche, M., & Paolucci, G. (2022). Synchrotron radiation investigation of archaeological metallic artifacts. *Journal of Synchrotron Radiation*, *29*, 532–539.

Abdellatief, M., Rebuffi, L., Khosroabadi, H., Najdawi, M., Abu-Hanieh, T., Attal, M., & Paolucci, G. (2017). High-energy X-ray studies of archaeological samples. *Powder Diffraction*, *32*(S1), S6–S12.

Azoor, R.M., Deo, R.N., Birbilis, N. and Kodikara, J. (2019). On the optimum soil moisture for underground corrosion in different soil types. *Corrosion Science*, *159*, 108116. https://doi.org/10.1016/j.corsci.2019.108116

Beale, T. W. (1973). Early trade in highland Iran: A view from a source area. World *Archaeology*, *5*(2), 133-148.

Chhabra, R., & Chhabra, R. (2021). Alkali soils, salt-affected soils and marginal waters: global perspectives and sustainable management. In: *Alkali Soils Salt-affected Soils and Marginal Waters: Global Perspectives and Sustainable Management*, pp.209–254.

Craddock, P.T., & Giumlia-Mair, A. (1988). Problems and possibilities for provenancing bronzes by chemical composition. *Bronzeworking Centres of Western Asia C*. 1000-539 BC. 317-326.

Dardeniz G. (2020). Why did the use of antimony-bearing alloys in Bronze Age Anatolia fall dormant after the Early Bronze Age?: A Case from Resuloğlu (Çorum, Turkey). PLoS ONE, *15*(7), e0234563. https://doi.org/10.1371/*journal.pone*.0234563

Dungworth, D. (2013). An experimental study of some early copper smithing techniques. In: D. Dungworth and RCP D, eds. *Accidental and Experimental Archaeometallurgy*. London: pp.149–152.

Fairservis, Walter Ashlin. (1961). Archaeological studies in the Seistan Basin of southwestern Afghanistan and eastern Iran. *Anthropological papers of the AMNH*; v. 48, pt. 1. https://www.biodiversitylibrary.org/bibliography/88438

Keykhaei, M., Haji Valiei, M., Shirazi, R., & Khademi Nadooshan, F. (2012). Shahr-i Sokhta and the bronze production workshop: A review. *Interdisciplinaria Archaeologica – Natural Sciences in Archaeology*, *3*(2), 203–210.

King, F. (2002). Corrosion of copper in alkaline chloride environments. [online] Available at: https://www.skb.com/publication/19607 [Accessed 4 Jul. 2025].

Kopezky, C.V., Novikov, V.Y., Fionova, L.K., & Bolshakova, N.A. (1985). Investigation of annealing twins in fcc metals. *Acta Metallurgica*, *33*(5), 873–879.

Lechtman, H., & Klein, S. (1999). The production of copper–arsenic alloys (arsenic bronze) by cosmelting: modern experiment, ancient practice. *Journal of Archaeological Science*, *26*(5), 497-526.

Moazzez Lesko, Z. and Sharifiyan Attar, R. (2002). *Mineralogy General*, Vol. 2. First ed. Tehran: [in Persian]. ISBN: 964-93722-2-9.

Panagiotaras, D., Papoulis, D. and Stathatos, E. (2015). Geochemistry of arsenic and toxic response. In: N. Chakrabarty, ed. *Arsenic Toxicity: Prevention and Treatment*. Boca Raton: CRC Press, Taylor and Francis, pp.79–109. ISBN: 9781482241969.

Pernicka, E. (2014). Provenance determination of archaeological metal objects. In Archaeometallurgy in global perspective: *Methods and syntheses* (pp. 239-268). New York, NY: Springer New York.

Philip, G., Clogg, P.W., Dungworth, D. and Stos, S. (2003). Copper metallurgy in the Jordan Valley from the third to the first millennia BC: Chemical, metallographic and lead isotope analyses of artefacts from Pella. *Levant*, *35*(1), 71–100. https://doi.org/10.1179/lev.2003.35.1.71.

Radivojević, M., Rehren, T., Kuzmanović-Cvetković, J., Jovanović, M., & Northover, J. P. (2013). Tainted ores and the rise of tin bronzes in Eurasia, c. 6500 years ago. *Antiquity*, *87*(338), 1030–1045. https://doi.org/10.1017/S0003598X0004984X

Rehren, T. (2003). Early Bronze Age copper metallurgy at Shahr-i Sokhta (Iran), reconsidered. In: Hauptmann, A. *et al.,* eds. *Man and Mining – Mensch und Bergbau. Studies in Honour of Gerd Weisgerber*, Der Anschnitt, Beiheft 16.

Robbiola, L., Blengino, J.M., & Fiaud, C. (1998). Morphology and mechanisms of formation of natural patinas on archaeological Cu–Sn alloys. *Corrosion Science*, *40*, 2083–2111.

Robotti, S., Rizzi, P., Soffritti, C., Garagnani, G. L., Greco, C., Facchetti, F., Borla, M., Operti, L., & Agostino, A. (2018). Reliability of portable X-ray fluorescence for the chemical characterisation of ancient corroded copper-tin alloys. *Spectrochimica Acta Part B: Atomic Spectroscopy, 146*, 41–49. https://doi.org/10.1016/j.sab.2018.04.017

Sajjadi, S.M.S., Foruzanfar, F., Shirazi, R., & Baghestani, S. (2003). Excavations at Shahr-i Sokhta. First preliminary report on the excavations of the graveyard, 1997–2000. *Iran*, 21–97.

Salvatori, S., & Tosi, M. (2005). Shahr-i Sokhta revised sequence. In: C. Jarrige and V. Lefèvre, eds. *South Asian Archaeology 2001*. Paris: Editions Recherches sur les Civilizations, pp.281–292.

Schmutzler, B., Eggert, G. and Kuhn-Wawrzinek, C.F. (2017). Copper (II) hydroxide on artefacts: Corrosion, conservation, colourants. *Studies in Conservation*, *62*(2), 61–67. Available at: https://www.jstor.org/stable/48544446

Scott, D.A. (1991). *Metallography and Microstructure of Ancient and Historic Metals*. Los Angeles, CA: Getty Conservation Institute.

Scott, D.A. (2002). *Copper and Bronze in Art: Corrosion, Colorants, Conservation*. Los Angeles, CA: Getty Conservation Institute.

Thornton, C. P., & Lamberg-Karlovsky, C. C. (2004). A new look at the prehistoric metallurgy of southeastern Iran. *Iran*, *42*(1), 47-59.

Thornton, C. P., & Roberts, B. W. (2009). Introduction: The beginnings of metallurgy in global perspective. *Journal of World Prehistory*, *22*(3), 181-184.

Tosi, M. (1984). The notion of craft specialization and its representation in the archaeological record of early states in the Turanian Basin. In: M. Spriggs, ed. *Marxist Perspectives in Archaeology*. Cambridge: pp.22–52.

Tylecote, R.F. (1979). The effect of soil conditions on the long-term corrosion of tin-bronze and copper. *Journal of Archaeological Science*, *6*, 345–368.

Weeks, L. (2012). *Early metallurgy of the Persian Gulf*: Technology, trade, and the Bronze Age world. Bril.